

Improper ferroelectricity in ultrathin hexagonal ferrites film

Xin Li,¹ Yu Yun,¹ Xiaoshan Xu^{1,2}*

¹Department of Physics and Astronomy, University of Nebraska, Lincoln, Nebraska 68588, USA

²Nebraska Center for Materials and Nanoscience, University of Nebraska, Lincoln, Nebraska 68588, USA

*Corresponding author: Xiaoshan Xu (X.X.)

Abstract:

The suppression of ferroelectricity in ultrathin films of improper ferroelectric hexagonal ferrites or manganites has been attributed to the effect of interfacial clamping, however, the quantitative understanding and related phenomenological model are still lacking. In this work, we report the paraelectric-to-ferroelectric phase transition of epitaxial h-ScFeO₃ films with different thickness through in-situ reflection high-energy electron diffraction (RHEED). Based on the interfacial clamping model and the Landau theory, we show that the thickness-dependence of the ferroelectric Curie temperature can be understood in terms of the characteristic length of interfacial clamping layer and the bulk Curie temperature. Furthermore, we found that the critical thickness of improper ferroelectricity is proportional to the characteristic length of interfacial clamping layer. These results reveal the essential role of mechanical clamping from interface on the improper ferroelectricity of hexagonal ferrites or manganites, and could serve as the guidance to achieve robust improper ferroelectricity in ultrathin films.

Introduction

The two-dimensional (2D) ferroelectricity has attracted intensive research interests recently due to novel mechanisms for stabilizing polar order as well as their great potentials to device scalability.^[1-3] In principle, epitaxial films of bulk ferroelectrics can also be scaled down to several unit cells. However, for proper ferroelectrics, such as BaTiO₃ (BTO), PbTiO₃ (PTO)^[4-8] of perovskite structures, if the depolarization field is not fully screened, there may exist critical thickness below which ferroelectricity is quenched. The critical-thickness problem can be absent in improper ferroelectrics. For example, in improper ferroelectric hexagonal manganites (h-RMnO₃, R=Sc, Y, Ho-Lu) or ferrites (h-RFeO₃), ferroelectric order originates from the linear coupling of polarization with non-polar structural distortion. This mechanism enables ferroelectricity in the ultrathin limit^[9-11], which is comparable to the range of thickness for 2D ferroelectricity.

On the other hand, recent studies revealed an interfacial clamping layer in hexagonal manganite and ferrite thin films^[9,10], which may affect the ferroelectricity significantly in the ultrathin limit. The transition temperature from paraelectric to ferroelectric phase was observed to decrease with reducing thickness and the interfacial clamping effect suppresses polarization within the first 2 unit cells (uc) in h-RMnO₃ film^[9]. Despite these observations, how the interfacial layer determines the temperature and thickness dependence of ferroelectricity has not been studied systematically, the ultrathin films of h-RFeO₃ could provide the chance to further clarify the general role of interfacial clamping layer.

Improper ferroelectric h-RFeO₃ is formed by triangle lattice of FeO₅ bipyramids sandwiched by rare earth layers^[11,12]. The triangle lattice of FeO₅ rotates 60 deg for alternative half unit cell, as shown in Fig.1 (a). The collective displacement of FeO₅ bipyramids corresponds to the K₃ mode distortion. The K₃ mode causes the imbalanced displacements of ions along the *c* axis (Γ_2^- mode), leading to the ferroelectricity in h-RFeO₃. The ferroelectricity is called improper since the primary order parameters are (Q, ϕ_Q), in which Q is the magnitude of in-plane displacement and ϕ_Q is the rotation angle of apical oxygen relative to the coordinates of FeO₅ bipyramids. The induced spontaneous polarization is proportional to $Q^3 \cos(3\phi_Q)$ in h-RFeO₃.

As shown in Fig.1(b), below T_c , the energy landscape of ferroelectric h-RFeO₃ is Mexican-hat shape with six-fold symmetry based on the Landau theory. For the ground states, the order parameter ϕ_Q can only take discrete values $\frac{n\pi}{3}$ where n is integer. When the temperature increases, the magnitude of Q for the ground states decrease gradually, which also leads to the suppression of polarization^[13]. Above T_c , the ferroelectric phase transforms to the paraelectric phase ($Q = 0$), as shown by in Fig.1(c) based on Landau theory^[14]. In addition to temperature-dependent phase transition, decreasing thickness is also expected to trigger the ferroelectric-to-paraelectric transition considering the interfacial clamping, as depicted in Fig.1(d). While the thermally driven transition is intrinsic to the temperature dependence of free energy, the thickness-driven transition is expected to be an extrinsic effect due to the elastic disruption of polar order at the film/substrate interface.

Here we focus on h-ScFeO₃ films, in which the smaller radius of Sc ion leads to stronger K₃ distortion with $Q \approx 1$ angstrom^[15,16]. We show that T_c of the h-ScFeO₃ films, inferred from

characteristic diffraction streaks of the in-situ RHEED patterns, decreases when the film thickness reduces. The thickness dependence of T_c and a critical thickness of ferroelectricity (ζ_{FE}) can be well modelled with the Landau theory using the characteristic length of the interfacial clamping layer (ζ_0) and the bulk Curie temperature (T_S) as two key parameters. These results elucidate that, in hexagonal ferrites and manganites, the interfacial-clamping-originated critical thickness is expected to affect scalability when it is comparable to the thickness of 2D ferroelectric layers.

Results and Discussion:

To reveal the origin of thickness-dependent scaling of T_c , the epitaxial h-ScFeO₃ films with different thickness were grown using pulsed laser deposition (PLD), followed by annealing at high temperature. The detailed growth conditions can be found in the previous work [15]. As shown in Fig. 2(a), the 2θ scans of x-ray diffractions indicate that h-ScFeO₃ films along the (0001) direction were formed on both Al₂O₃ (0001) and SrTiO₃ (STO)(111) substrates without impurity phase. Moreover, the in-plane epitaxy relationship can be inferred by comparing the RHEED patterns of film with substrate in Fig. 2(b). Specifically, the in-plane [100] direction of h-ScFeO₃ film is parallel to $[\bar{1}1\bar{2}0]$ of Al₂O₃ and $[\bar{2}11]$ of STO, respectively.

In h-RFeO₃, paraelectric-to-ferroelectric phase transition is accompanied by the tripling of the in-plane unit cell for the ferroelectric phase (P6₃cm) compared with the paraelectric phase (P6₃/mmc), as indicated in Fig. 1(d). Since the separation of the RHEED streaks is inversely proportional to the in-plane lattice constant^[17-19], RHEED patterns with the electron beam along the h-ScFeO₃ [100] direction provides a measurement for tripled unit cell of ferroelectric phase with P6₃cm symmetry. Specifically, the RHEED pattern of the paraelectric phase consists of the (0,0) and ($\pm n,0$) diffraction streaks. The tripled in-plane unit cell of the ferroelectric phase leads to the formation of weaker diffraction streaks at the $\pm(3n+1)/3$ and $\pm(3n+2)/3$ positions along h-ScFeO₃ [001] direction, as shown in Fig. 2(b).

Fig. 3(a) to (c) display two-dimensional RHEED patterns of 2, 5 and 17 unit cell (uc) h-ScFeO₃/Al₂O₃ films respectively, which were captured at room temperature, below which are the normalized line profiles of RHEED intensity after integrated along vertical direction, with background subtracted. For the 17 uc film, the intensity of the weak streaks gradually increases when the temperature decreases, indicating the existence of thermal driven paraelectric-to-ferroelectric phase transition. When the thickness is 2 uc, as shown in Fig. 3(a), no weak streaks could be identified down to the room temperature. The missing weak streaks suggests that the mechanical boundary conditions at the interface, or interfacial clamping, modifies the energy-minimum state and fully suppress the K₃ distortion in the interfacial layers.

To trace the change of T_c with respect to the film thickness, the temperature dependence of RHEED intensity of the weak streaks was analyzed quantitatively. Fig. 4 shows the intensity of the weak streaks, normalized using the (1,0) and (-1,0) streaks, as a function of temperature for various film thickness for h-ScFeO₃ films grown on both Al₂O₃ and STO substrates. As shown in Fig. 4(a), there is no obvious transition for the intensity of the weak streak for the 2 uc film, so the ferroelectric T_c may be lower than the room temperature. All the other films, with thickness

ranging from 4 to 41 uc, exhibit a transition of the weak streak intensity above room temperature. More importantly, T_c increases when the thickness increases.

To interpret the key factors determining the thickness-dependent scaling of T_c in ultrathin h-RFeO₃ film and the potential critical thickness, we treat the h-RFeO₃ near the interface as interfacial clamping layer, where the magnitude of structural distortion (Q) is suppressed completely at the beginning, and increases gradually when rare earth layer is away from the interface^[10,11]. Considering the free energy of the structural distortion and the elastic energy at the same time within the framework of Landau theory^[14,20] (see details in supplementary), the structural distortion with thickness and temperature can be written analytically as:

$$Q(z, T) = Q_\infty(T) \frac{1 - \exp\left(-\frac{z}{\zeta(T)}\right)}{1 + \exp\left(-\frac{z}{\zeta(T)}\right)}, \text{ with } \begin{cases} Q_\infty(T) = \sqrt{\frac{-a_0}{b}} \sqrt{1 - \frac{T}{T_s}} = Q_0 \sqrt{1 - \frac{T}{T_s}} \\ \zeta(T) = \sqrt{\frac{k}{-a_0}} \sqrt{\frac{T_s}{T_s - T}} = \zeta_0 \sqrt{\frac{T_s}{T_s - T}} \end{cases} \quad (1)$$

in which $a_0 < 0$ and $b > 0$ are coefficients of Landau theory, k corresponds to stiffness coefficient, T_s is the Curie temperature of bulk state, and ζ_0 is the characteristic length of interfacial clamping layer at $T = 0$ K. By integrating the energy density with the thickness of ferroelectric layer (t_F), the total energy can be expressed as:

$$F(t_F, T) = -\frac{a_0}{2T_s} C1(t_F, T) \left\{ \left[T - \left(T_s + \frac{2kT_s}{a_0} \frac{C2(t_F, T)}{C1(t_F, T)} \right) \right] Q_\infty(T)^2 + \frac{T_s}{2*Q_0^2} \frac{C3(t_F, T)}{C1(t_F, T)} Q_\infty(T)^4 \right\} \quad (2)$$

with

$$\begin{cases} C1(t_F, T) = \int_0^{t_F} \left(\frac{1 - \exp\left(-\frac{z}{\zeta(T)}\right)}{1 + \exp\left(-\frac{z}{\zeta(T)}\right)} \right)^2 dz \\ C2(t_F, T) = \int_0^{t_F} \frac{\left(\frac{2}{\zeta} * \exp\left(-\frac{z}{\zeta(T)}\right) \right)^2}{\left(1 + \exp\left(-\frac{z}{\zeta(T)}\right) \right)^4} dz \\ C3(t_F, T) = \int_0^{t_F} \left(\frac{1 - \exp\left(-\frac{z}{\zeta(T)}\right)}{1 + \exp\left(-\frac{z}{\zeta(T)}\right)} \right)^4 dz \end{cases} \quad (3)$$

When the coefficient before $Q_\infty(T)^2$ term is less than zero, minimizing $F(t_F, T)$ results in finite $Q_\infty(T)$ corresponding to the ferroelectric order. At $T = T_c$, this coefficient is zero, i.e.,

$$\alpha(t_F, T) = T - T_s \left[1 - 2\zeta_0^2 \frac{C2(t_F, T)}{C1(t_F, T)} \right] = 0 \quad (4)$$

(see details in supplementary).

The phase diagram of $\alpha(t_F, T)$ for h-ScFeO₃ films is plotted in Fig. 5(a), with ζ_0 and T_S inferred in Fig.5(b). Since $\alpha(t_F, T) < 0$ (> 0) corresponds to the ferroelectric (paraelectric) state of the h-RFeO₃ films, the curve of $\alpha(t_F, T) = 0$ indicates that the critical thickness of ferroelectricity increases with temperature, which is consistent with the observation of temperature-dependent corrugation of rare earth layers in h-YMnO₃/YSZ film^[10]. Moreover, as implied by Eq. (4), the dependence of T_c on t_F is influenced by both T_S and ζ_0 , which are two independent parameters that can be extracted from experimental observations, such as in-situ RHEED patterns in this work. As shown in Fig. 5(b), the experimental T_c of both h-ScFeO₃ and h-YMnO₃ films decreases with smaller thickness, and the trend is slower in the h-ScFeO₃ films. By fitting the experimental data with Eq. (4), we find for h-YMnO₃/YSZ film, that $T_s = 814 \pm 183$ K and $\zeta_0 = 0.93 \pm 0.44$ uc. For the h-ScFeO₃ films, we find $T_s = 681 \pm 28$ K and $\zeta_0 = 0.68 \pm 0.18$ u.c. Therefore, the slower suppression of T_c with thickness in h-ScFeO₃ films can be attributed to smaller ζ_0 .

It should be noted that the phenomenological model here does not consider the transition of single domain to multi-domain states with thickness, since the elastic energy is much larger than depolarization energy^[13], as well as possible variation of stiffness constant at the interface, which may contribute to the minor discrepancy. Moreover, based on Eq. (4), the ferroelectric critical thickness (ζ_{FE}) can be defined as the interception of $\alpha(t_F, T) = 0$ with $T = 0$ K, as shown in Fig.5 (c), and the ratio of $\zeta_{FE}/\zeta_0 = 2.25$ is a fixed value, which is independent of materials (see details in supplementary Section 3). This ratio indicates that the absence of ferroelectric critical thickness ($\zeta_{FE} = 0$) or unsuppressed corrugation of initial rare-earth layer in h-RFeO₃ or h-RMnO₃ films can only exist when there is no interfacial clamping layer ($\zeta_0 = 0$) or when the films become freestanding. Moreover, the improper ferroelectricity under ultrathin limit could be artificially controlled by choosing the characteristic length of interfacial clamping layer through different interface.

Conclusion

In summary, through quantitative study of in-situ RHEED patterns during paraelectric-to-ferroelectric phase transition, the thickness-dependent scaling of ferroelectric T_c in epitaxial h-ScFeO₃ films was revealed for the first time. Based on interfacial clamping layer, a phenomenological model from Landau theory was introduced to interpret this scaling behavior and reveal the correlation between ferroelectric critical thickness and characteristic length of interfacial clamping layer in ultrathin h-RFeO₃ or h-RMnO₃ film. These results serve as the guidance to achieve robust improper ferroelectricity in h-RFeO₃ through interfacial engineering for future study.

Experimental section

The h-ScFeO₃/Al₂O₃ (0001) and h-ScFeO₃/SrTiO₃ (111) epitaxial thin films were grown using pulsed laser polarization (PLD) with base pressure lower than 3×10^{-7} mTorr, a repetition rate of 2 Hz. Before the deposition, the substrates were pre-annealed at 700 °C for 1 hour. During the growth, the substrate temperature was kept at 700 °C - 920 °C, specifically, the films were grown at low temperature first (~ 700 °C) then annealed at high temperature (~ 920 °C). The growth

oxygen pressure is 10 mTorr. The in-situ RHEED was used to monitor ferroelectric to paraelectric phase transition of h-ScFeO₃ film after the growth, the incident angle of electron beam is kept fixed during the process of reducing temperature, and the raw images of RHEED are analyzed based on python program. The crystal structure and the thickness of the epitaxial h-ScFeO₃ films were measured by XRD (Rigaku SmartLab Diffractometer).

Acknowledgements

Funding: This work was primarily supported by the National Science Foundation (NSF), Division of Materials Research (DMR) under Grant No. DMR-1454618 and by the Nebraska Center for Energy Sciences Research. The research was performed in part in the Nebraska Nanoscale Facility: National Nanotechnology Coordinated Infrastructure and the Nebraska Center for Materials and Nanoscience, which are supported by the NSF under Grant No. ECCS- 2025298, and the Nebraska Research Initiative.

Reference:

1. M. Osada, T. Sasaki. *APL Mater.* 7, 120902 (2019)
2. C. Cui, F. Xue, W.-J. Hu, L.-J. Li. *Npj 2D Mater. Appl.* 2, 18 (2018).
3. M. Wu, P. Jena. *Wiley Interdiscip. Rev. Comput. Mol. Sci.* 8, e1365 (2018).
4. D. D. Fong, G. B. Stephenson, S. K. Streiffer, J. A. Eastman, O. Auciello, P. H. Fuoss, C. Thompson. *Science* 304, 1650–1653 (2004).
5. D. D. Fong, A. M. Kolpak, J. A. Eastman, S. K. Streiffer, P. H. Fuoss, G. B. Stephenson, Carol Thompson, D. M. Kim, K. J. Choi, C. B. Eom, I. Grinberg, and A. M. Rappe. *Stabilization of Monodomain Polarization in Ultrathin PbTiO₃ Films.* *Phys. Rev. Lett.* 96, 127601(2006).
6. Jia, CL., Nagarajan, V., He, J. Q. et al. *Nature Mater* 6, 64–69 (2007).
7. Junquera, J., Ghosez, P. *Nature* 422, 506–509 (2003).
8. Y. S. Kim, D. H. Kim, J. D. Kim, Y. J. Chang, and T. W. Noh. *Appl. Phys. Lett.* 86, 102907 (2005)
9. N. Sai, C. J. Fennie, A. A. Demkov. *Phys. Rev. Lett.* 102, 107601(2009).
10. J. Nordlander, M. Campanini, M. D. Rossell, et al. *Nat. Commun* 10, 5591 (2019).
11. Y. Yun, et al. *Spontaneous Polarization in an Ultrathin Improper-Ferroelectric/Dielectric Bilayer in a Capacitor Structure at Cryogenic Temperatures.* *Phys. Rev. Applied* 18, 034071(2022)
12. X. Li, Y. Yun. et al. *Domain-wall magnetoelectric coupling in multiferroic hexagonal YbFeO₃ films.* *Sci. Rep* 13, 1755 (2023).

13. M. Lilienblum, T. Lottermoser, S. Manz, et al. Ferroelectricity in the multiferroic hexagonal manganites. *Nature Phys* 11, 1070–1073 (2015).
14. Artyukhin, S., Delaney, K., Spaldin, N. et al. *Nature Mater* 13, 42–49 (2014).
15. Ki. Sinha, H. Wang, X. Wang, L. Zhou, Y. Yin, W. Wang, X. Cheng, D.J. Keavney, H. Cao, Y. Liu, X. Wu, X. Xu. *Phys. Rev. Lett.* 121, 237203 (2018).
16. X. Xu, W. Wang. Multiferroic hexagonal ferrites (h-RFeO₃, R = Y, Dy-Lu): A brief experimental review. *Mod. Phys. Lett. B* 28, 1430008 (2014).
17. A. Ichimiya, P. I. Cohen. *Reflection High Energy Diffraction*. Cambridge University Press.
18. W. Wang, J. Zhao et al. Room-Temperature Multiferroic Hexagonal LuFeO₃ Films. *Phys. Rev. Lett.* 110, 237601 (2013)
19. X. Zhang et al. Effect of interface on epitaxy and magnetism in h-RFeO₃/Fe₃O₄/Al₂O₃ films (R = Lu, Yb). *J. Phys.: Condens. Matter* 29, 164001 (2017).
20. C. X. Zhang, K. L. Yang, P. Jia, H. L. Lin, C. F. Li, L. Lin, Z. B. Yan, J.-M. Liu. *J. Appl. Phys.* 123, 094102 (2018).

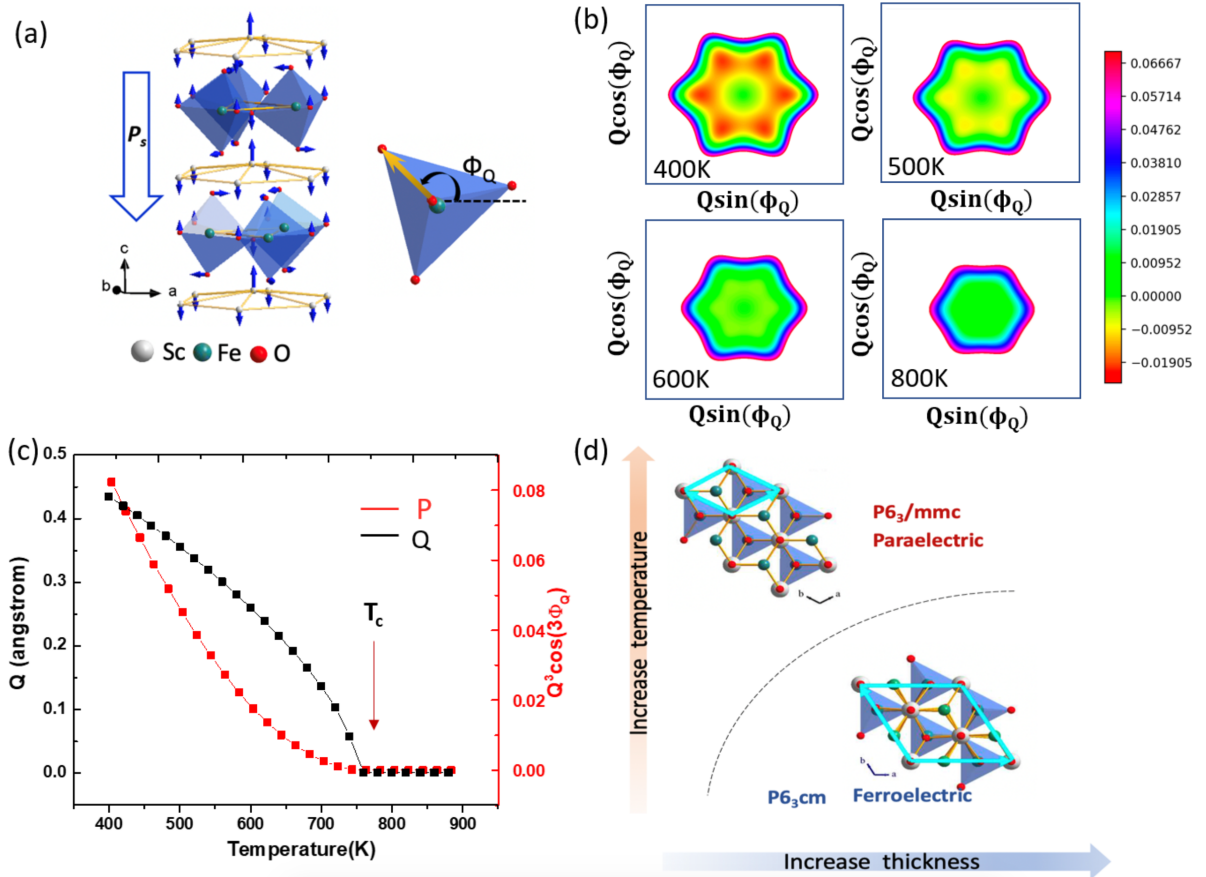


Fig.1 (a) Atomic structure of h-RFeO₃ and the rotation angle of apical oxygen atoms (ϕ_Q). (b) Representative energy landscapes of h-RFeO₃ at different temperature, assuming T_c as 750 K. (c) The schematic diagram for the temperature dependence of the order parameter Q and the polarization $P=Q^3\cos(3\phi_Q)$ for bulk-state h-RFeO₃, based on the Landau theory. (d) Schematic diagrams for the temperature and thickness driven phase transition in h-RFeO₃ films and related atomic structures in a-b plane.

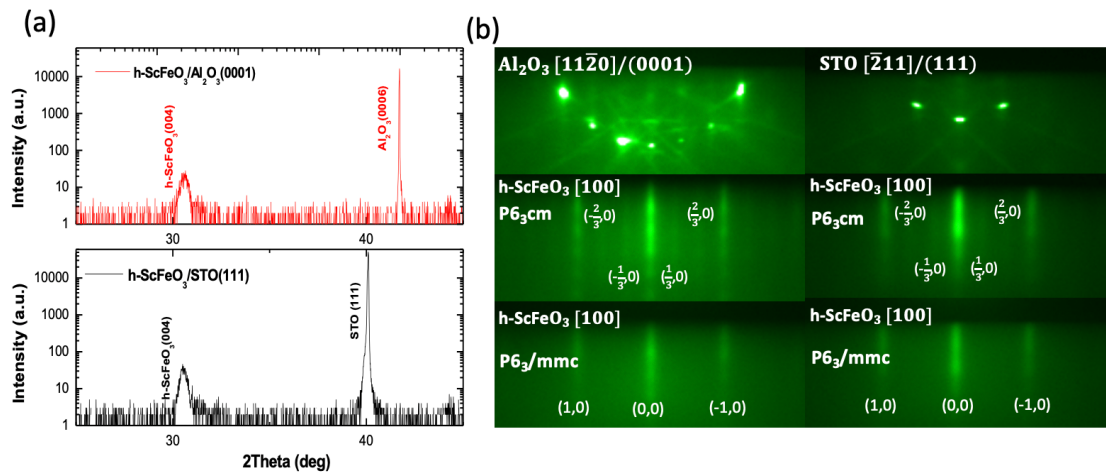


Fig.2 (a) 2θ scan for h-ScFeO₃/Al₂O₃ and (b) h-ScFeO₃/STO films. (b) RHEED patterns of ferroelectric phase (P6₃cm symmetry) and paraelectric phase (P6₃/mmc symmetry) and in-plane epitaxy relationships for h-ScFeO₃/Al₂O₃ and h-ScFeO₃/STO films.

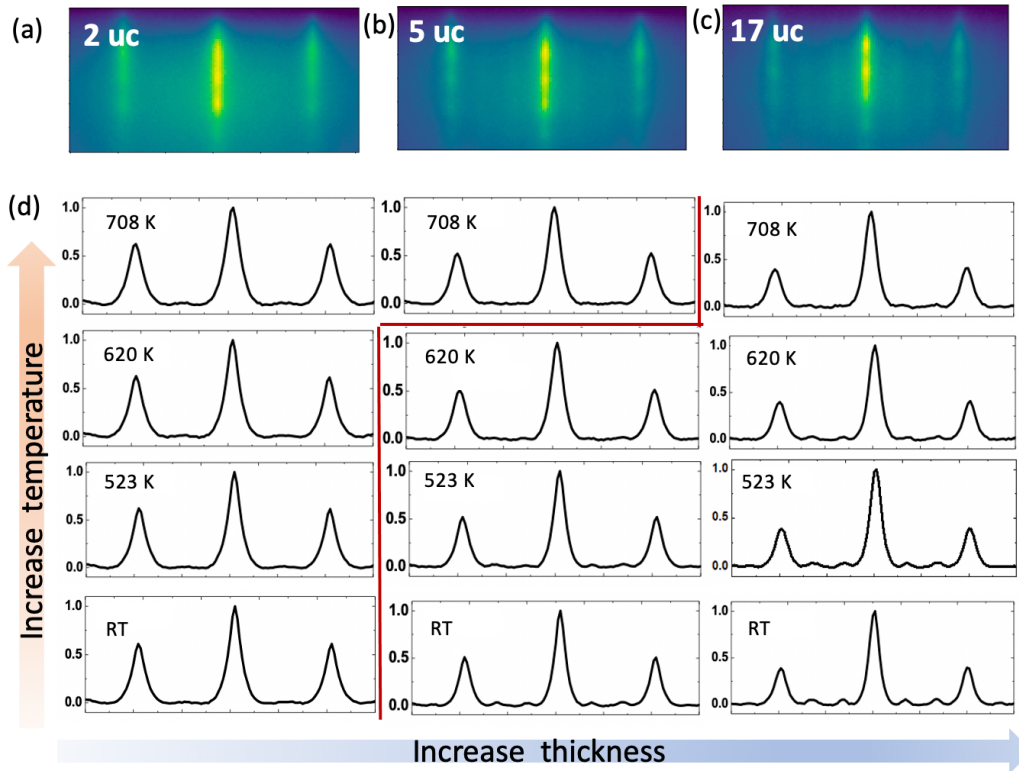


Fig.3 (a) to (c) RHEED images of h-ScFeO₃/Al₂O₃ films with thickness of 2, 5, 17 uc at room temperature. (d) Normalized profiles of RHEED intensity with different thickness and temperature for h-ScFeO₃/Al₂O₃ films.

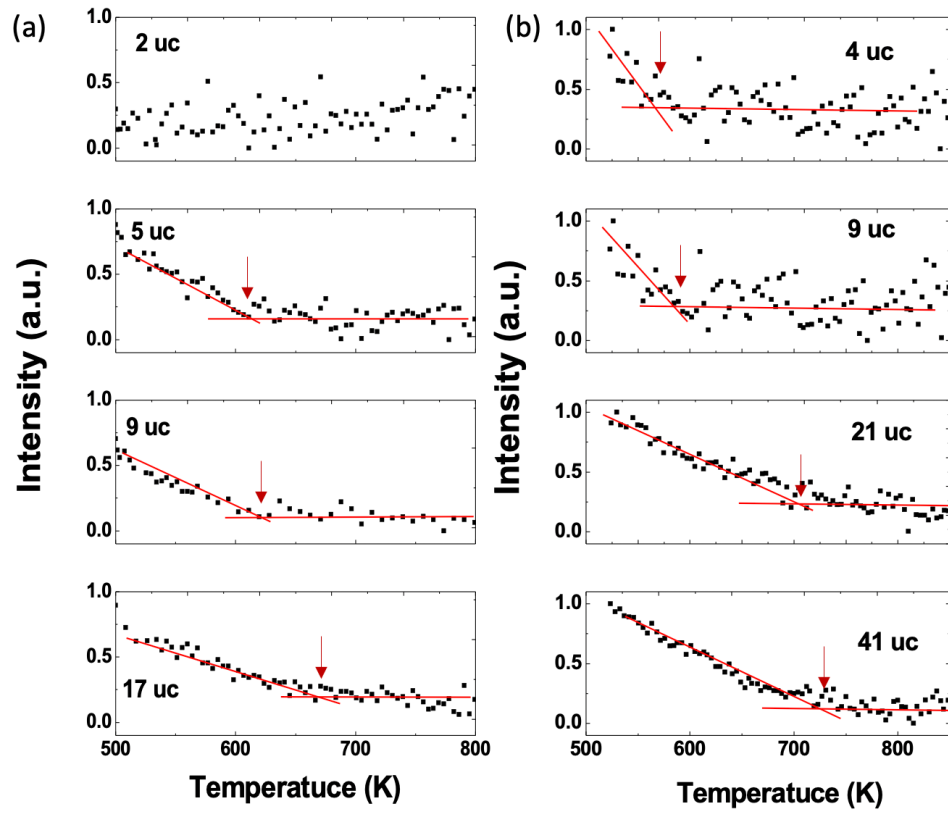


Fig.4 Normalized RHEED intensity of $(1/3, 0)$ streak with temperature for (a) $h\text{-ScFeO}_3/\text{Al}_2\text{O}_3$ and (b) $h\text{-ScFeO}_3/\text{STO}$ films with different thickness.

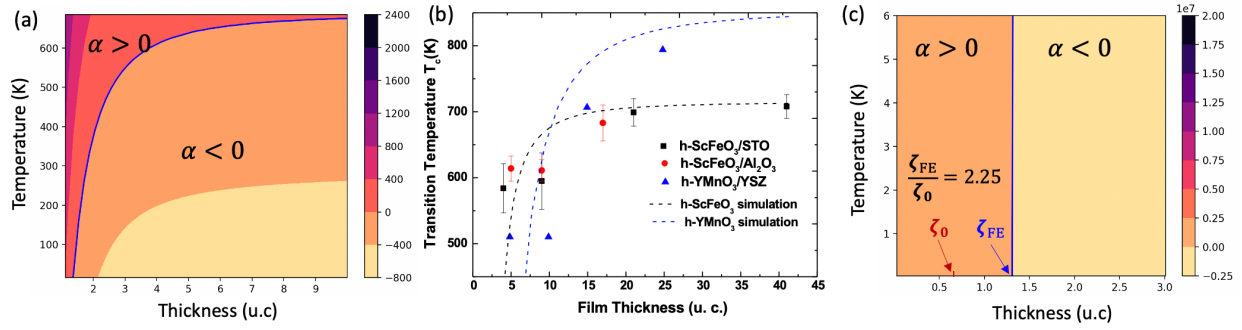


Fig.5 (a) Calculated phase diagram of coefficient α in Eq. (4) with temperature and film thickness as independent variables, the blue solid blue line corresponds to $\alpha = 0$. (b) Measured thickness-dependent T_c of h-ScFeO₃/STO, h-ScFeO₃/Al₂O₃ and h-YMnO₃/YSZ films and related fitting based on Eq. (4), the data of h-ScFeO₃ comes from in-situ RHEED in this work and the data of h-YMnO₃ comes from Ref. [9]. (c) Phase diagram of α near $T = 0$ K and the comparison of ζ_0 and ζ_{FE} .